DEVELOPMENT OF 600MPA GRADE HIGH DUCTILITY HOT-ROLLED SHEET STEEL FOR AUTOMOTIVE SQUARE TUBE*

Yajun Hui[1]
Kun Liu[2]
Hui Pan[3]
Baoliang Xiao[4]
Dawei Zhang[5]
Fengxia Bai[6]

Abstract

The microstructure, properties, strengthening mechanism and work hardening mechanism of 600MPa grade high ductility hot-rolled sheet steel for automotive square tube were investigated by utilizing optical microscopy, scanning electron microscopy and transmission electron microscopy. The results show that the microstructures of low C-low Mn-Nb and Ti microalloyed steel (Steel A) and high C-high Mn-Nb microalloyed steel (Steel B) are composed of ferrite and a small amount of pearlite. Compared with steel B, the size of ferrite and pearlite of steel A is finer, while the size of the second phase precipitates is larger. The mechanical properties of the two tested steels are similar before tube forming, except that the yield ratio of steel A is higher. Steel A has/exhibits significant work hardening after tube forming; the yield strength and tensile strength increase by 45 MPa and 26 MPa, respectively, while the elongation decrease by 6.0 percent. The yield strength and tensile strength of steel B increase by 22 MPa and 10 MPa, respectively, and the elongation decrease by 4.0 percent. The grain refinement strengthening is the dominant strengthening mechanism, accounting for 52.9 to 61.8 percent of the total yield strength; the solid solution strengthening is the second strengthening mechanism, accounting for 17.2 to 25.3 percent, while the precipitation strengthening and dislocation strengthening contribute little to the yield strength. The dislocation strengthening increase by 82 MPa of steel A after tube forming, which is higher than that of steel B. Therefore, steel B has a low work hardening rate that is more suitable for manufacturing automotive square tube for secondary tube forming.

Keywords: 600MPa grade, Square tube steel; Strengthening mechanism; Work hardening mechanism.

[1] *Master, Engineer, Sheet Metal Research Institute, Technology Institute of Shougang Group Co., Ltd., Beijing, China.*
[2] *Doctor, Senior engineer, Sheet Metal Research Institute, Technology Institute of Shougang Group Co., Ltd., Beijing, China.*
[3] *Master, Senior engineer, Sheet Metal Research Institute, Technology Institute of Shougang Group Co., Ltd., Beijing, China.*
[4] *Doctor, Engineer, Sheet Metal Research Institute, Technology Institute of Shougang Group Co., Ltd., Beijing, China.*
[5] *Master, Engineer, Sheet Metal Research Institute, Technology Institute of Shougang Group Co., Ltd., Beijing, China.*
[6] *Doctor, Engineer, Sheet Metal Research Institute, Technology Institute of Shougang Group Co., Ltd., Beijing, China.*

1 INTRODUCTION

In response to the pressure of oil energy consumption and exhaust emission pollution caused by the development of automobile industry, China has released the “Technology Roadmap for Energy Saving and New Energy Vehicles” in 2016. It stipulated that the average fuel consumption of commercial vehicles will be 10 percent lower in 2020 than that in 2015, 15 percent lower in 2025, and 20 percent lower in 2030[1]. The rapid development of electric vehicles and hybrid vehicles in recent years greatly reduced automobile exhaust pollution. With battery serves as the energy source of vehicle, its weight determines the endurance of battery. Therefore, whether it is for fuel vehicles or electric vehicles, lightweight has an important economic and social values [2]. Automotive lightweight could be achieved by using lightweight materials, advanced processes and structural optimization. Among these methods, application of lightweight materials is the mainstream [3-4]. At present, new materials mainly include high strength steel, aluminum alloy, magnesium alloy, composite materials and engineering plastics. The production process of aluminum alloy is mature, but the bearing capacity and mechanical properties is not good compared with steels. Magnesium alloy has low density, but it is expensive, and the carbon emission is high throughout its life cycle. The plastic products are light and easy to process, but there are environmental pollution problems in the recycling process, which limits its use. Carbon fiber materials have the best weight reduction effect, but they are expensive and difficult to process. Compared with the above-mentioned materials, high strength steels show attractive advantages. Applying high strength steels can not only reduce component size and structure quality, save steel consumption, reduce the cost of processing and transportation, but also achieve higher stability than low strength steels [5-8].

At present, it is widely believed that the exhaust emission of vehicles is one of the main sources of smog. From 2015 to 2017, the annual sale of bus in China is more than 500,000. The weight of ordinary bus with 50 seats reaches 12 tons, which have higher fuel consumption and exhaust emission than passenger cars. The body skeleton is the main load-bearing structure, accounting for about 30 percent of the total weight. Most of the square tubes used on the body frame are manufactured by Q235 and/or Q345; by using high strength square tubes instead of low strength ones can significantly reduce the weight, which is the development trend of high-end bus in the future [9]. Due to control the rebound of high strength steels difficultly, combined with the deterioration of plasticity caused by the complex plastic deformation during tube rolling process, the application of square tube manufactured by high strength steels is limited.

In this work, in order to determine the composition design that is more suitable for manufacturing automotive square tube for secondary tube forming, the microstructure and properties of 600MPa high ductility hot rolled sheet steel for automotive square tube with different chemical compositions were studied by optical microscopy (OM), scanning electron microscopy (SEM) and transmission electron microscopy (TEM).

2 MATERIAL AND METHODS

The chemical compositions of 600MPa high ductility hot rolled sheet steels for automotive square tube are shown in Table 1. Steel A was microalloyed by niobium and titanium with low content of carbon and manganese, steel B was microalloyed by niobium with high content of carbon and manganese.

Table 1. Chemical composition of 600MPa high ductility hot rolled sheet steel for automotive square tube（mass fraction, %）

Steel	C	Si	Mn	P≤	S≤	Alt	Nb	Ti
A	0.06	0.15	1.1	0.020	0.008	0.025	0.03	0.03
B	0.12	0.15	1.4	0.020	0.008	0.025	0.03	

The ingots were homogenized at 1230 ℃ for 200 min and hot rolled to 3 mm thick with the finishing rolling temperature of 880 ℃ . The finished steel plates were subsequently cooled to 590~620 ℃. Then the steel plates was rolled into a square tube with the size of 40 mm × 40 mm.

Tensile specimens with the gage length of 50 mm and width of 12.5 mm were machined from hot rolled steel plates and the surface of square tube along the rolling direction. Tensile tests were performed at room temperature with a constant crosshead speed of 2 mm/min according to GB/T 228-2002.

Samples for microstructure observation were cut from hot rolled steel plates and the surface of square tube, then mechanically polished and etched in 5 percent nital solution. MEF4A optical microscope and S3400N scanning electron microscope were used to observe the microstructure and the average diameter of ferrite grains.

TEM studies were carried out on the thin foils and carbon extraction replicas. The thin foil samples were prepared from 0.30 mm thick disks sliced from hot-rolled steel plates. The disks were thinned to 0.05 mm by abrasion on SiC papers and then twin-jet electro-polished using a solution containing 5 percent perchloric acid, 5 percent glycerol, and 90 percent ethanol at a temperature of -17.5 ℃ and a voltage of 45 V. The carbon extraction replicas were prepared by grinding and polishing the samples to 1 μm. The surface was etched with 3 percent nital, and the carbon was evaporated onto the etched surface. Finally, the surface was scored into about 2 mm squares, and the sample was etched in 3 percent nital with a stainless steel cathode to remove the replica. The extracted carbon replicas were then rinsed with water and alcohol mixture, and then placed on the copper grid and dried. A JEM-2000FX transmission electron microscope was used to observe nanometer sized carbides, assisted with the use of a nanometer probe energy dispersive spectrometer. Moreover, the dislocation was observed by foils samples and the dislocation density was calculated [10, 11].

3 RESULTS AND DISCUSSION

3.1 Mechanical properties

Table 2 shows the mechanical properties of 600MPa high ductility hot rolled sheet steel for automotive square tube before and after tube forming. It can be seen that the mechanical properties of the tested steels had met the technical requirement before tube forming. The yield strength, tensile strength and elongation of steel A are 540 MPa, 607 MPa and 29.5 percent, respectively, and the yield ratio is 0.89. The above indexes of steel B are 530 MPa, 624 MPa and 30.5 percent, respectively, the yield ratio is 0.85. The yield strength of steel B is 10 MPa lower than steel A and the tensile strength is 17 MPa higher. The hot rolling process parameters are the same for both steel A and steel B, the obvious difference in their mechanical properties is caused by different chemical compositions.

For the mechanical properties after tube forming of the tested steels, the yield strength, tensile strength, elongation and yield ratio of steel A are 585 MPa, 636 MPa, 23.5 percent and 0.92, respectively. Compared with the mechanical properties of steel A before tube forming, the yield strength and tensile strength increased by 45 MPa and 26 MPa, respectively, while the elongation decreased by 6.0 percent which was unable to meet the requirement. The yield strength, tensile strength, elongation and yield ratio of steel B after tube forming are 552 MPa, 634 MPa, 26.5

percent and 0.87, respectively. The yield strength and tensile strength increased by 22 MPa and 10 MPa, respectively, and the elongation decreased by 4.0 percent. Both the strength and the elongation could meet the requirements.

Comparing the change of mechanical properties of the tested steels before and after tube forming, it can be seen that steel A has a significant work hardening during tube forming, much higher than that of steel B. The tensile strength of the tested steels after tube forming are similar, while the yield strength of steel A is higher and its elongation is lower. Since the square tube may still need to roll in the subsequent use, it is prone to crack when the elongation of the square tube is low. Therefore, steel B is more suitable for manufacturing square tube.

Table 2. Mechanical properties of 600MPa high-ductility automotive square tube steel before and after tube forming

Steel	Note	Rel/Mpa	Rm/Mpa	A/%
A	Plate	540	607	29.5
	Tube	585	636	23.5
B	Plate	530	624	30.5
	Tube	552	634	26.5
Requirement	Plate	⩾500	⩾600	⩾28.0
	Tube	⩾500	⩾600	⩾24.0

Rel: Yield strength; Rm: Tensile strength; A: Elongation

3.2 Microstructure of steel plates

Figure 1 shows the OM images of the tested steels. The microstructures of both tested steels are composed of ferrite (bright areas) and a small amount of pearlite (dark areas). The average grain size of steel A is about 2.6 μm, with a grain grade of 14.0. The shape of the pearlite pellets is irregular, which distributed in the grain boundaries of the ferrite in blocks or strips. The average size of the pearlite pellets is about 1.30 μm, and the volume fraction of pearlite pellets is about 5.52 percent. There are many carbides in the grain boundary and inside of the ferrite, as shown in Figure 1(a). The average grain size of steel B is about 3.7 μm, which is obviously larger than that of steel A. The pearlite pellets are also in the shape of blocks and strips. The size of pearlite pellets reaches 2.32 μm, with a volume fraction of about 7.86 percent. Both the size and the volume fraction of pearlite pellet of steel B are larger than steel A, as shown in Figure 1(b).

Under the same production process, the size of ferrite in steel A is smaller than that of steel B, which is affected by the composition. Steel A has a lower carbon content and is microalloyed by Niobium and Titanium. Compared with steel B, the austenitizing temperature of steel A is higher, and the carbonitrides of Niobium and Titanium, which can pin the austenite grains to suppress their growth, have higher full solution temperatures. Therefore, the original austenite grain size of steel A is smaller than that of steel B. Moreover, the carbonitites of Niobium and Titanium is re-precipitated during rolling process, which can hinder the recovery of recrystallization and the growth of the austenite to supply more nucleation sites. As mentioned above, the ferrite grain size of steel A is smaller than that of steel B.

The pearlite transformation is a diffusive transition, and the pearlite transformation kinetics is affected by the diffusion of carbon and alloying elements. For hypoeutectoid steel, the pearlite transformation is promoted with the increase of carbon content. For the alloying elements, the carbonitride-tube forming element would slow down the dynamics of the pearlite transformation, especially Nb, V, and Ti element. The pearlite content of steel B is higher than that of steel A because of the higher content of carbon and the lower content of microalloying elements. The pearlite formation temperature and the original austenite grain size affect the size of pearlite pellet. Since steel B has a higher pearlite formation temperature and larger original austenite grain size than steel A, the size of pearlite pellets is larger.

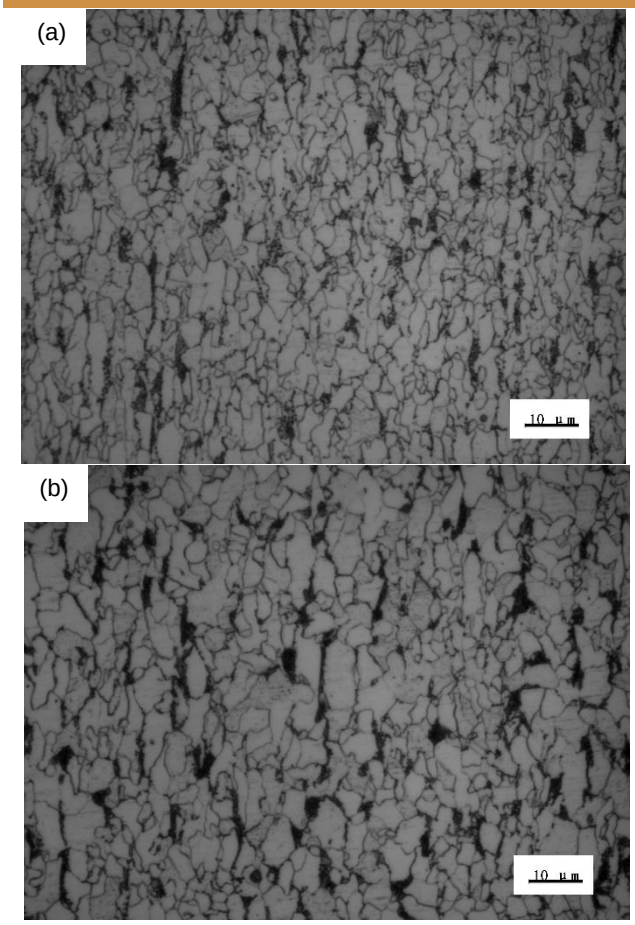

Figure 1. OM images of the hot rolled steel plate (a) steel A; (b) steel B.

3.3 Microstructure of the square tube

The microstructure of welding position of the square tube manufactured by steel B is shown in Figure 2. It can be seen in Figure 2(a) that there is a bright band fusion line in the center of weld, and the metal on both sides has a streamlined shape along the fusion line. In high-frequency induction welding, the metal at the center of the weld is firstly heated to molten state, and the molten metal are fused under pressure, a partially metal in molten state is extruded into the weld to form a streamlined shape. The metal at the center of the weld undergoes high temperature, combined with the fact that it exposes as surface, oxidative decarburization would occur and result in coarse austenite grains. In addition, due to the high heating temperature and the dissolution of carbonitride into austenite, austenite grains will abnormally coarsen. Lamellar bainite or acicular ferrite is formed with a small amount of granular bainite under rapid cooling after welding, thus leading to a significant drop in ductility and impact toughness. The heat affected zone is heated to a range of Ac3 to 1200 ℃. The ferrite and pearlite are all austenitized. Because of high heating speed and short residence time at high temperature of high-frequency induction welding, the austenite grains are fine, so that the microstructure of the heat affected zone is uniformly composed with fine ferrite with a small amount of pearlite, leading to a good ductility and toughness. With the gradual increase of the distance from the weld center, the heat-affected zone change from complete recrystallized zone to incomplete recrystallized zone, and the ferrite grains gradually coarsen. The microstructure of the base metal in the plane face of the square tube is mainly the mixed structure of ferrite and pearlite, which is almost the same with the hot rolled strip before roll tube forming. The metal has undergone a complex plastic deformation during manufacturing square tube, the yield strength increases and the elongation decreases, which are mainly caused by the increase of dislocation density and the change of microstructure. While the change of mechanical properties of the weld position is mainly caused by the change of microstructure, the occurrence of bainite makes the yield strength and tensile strength increase, and the elongation decrease. In order to meet the requirement of further deformation for manufacturing square tube, the weld microstructure should be mainly bainite, avoiding martensite, and the heat affected zone should be mainly composed of recrystallized ferrite.

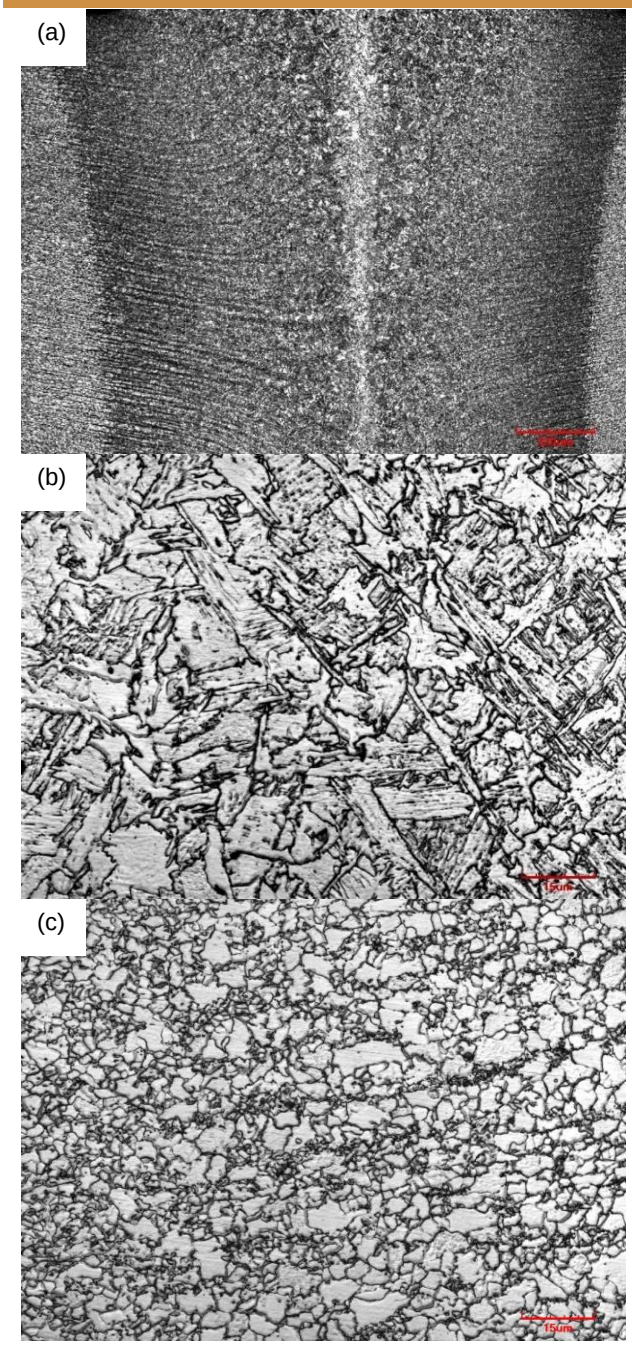

Figure 2. Microstructure/OM images of different weld positions of the square tube manufactured by steel B (a) macroscopic morphology of weld position; (b) center of the weld; (c) heat affected zone.

3.4 The second phase precipitate

TEM images of the second phase precipitates of the tested steels are shown in Figure 3. The size distribution of the second phase precipitate is shown in Figure 4. Both the morphology and the size of the second phase precipitates of the test steels with different compositions are significantly different. The shape of the second phase precipitates of steel A includes cubic, spherical, ellipsoidal, etc. The size of the second phase precipitates distributes between 3 nm and 120 nm, and the average size is 61 nm. The energy spectrum analysis shows that they are (Nb, Ti) C, with relatively high Ti content, as shown in Figure 3(a) and (b). The second phase precipitates distributed between 20 and 90 nm account for 86.0 percent. Those below 20 nm and above 90 nm account for 7 percent.

The morphology of the second phase precipitates of steel B is spherical and ellipsoidal, and the size mainly distributes between 1nm and 100nm, the average value is about 44nm, which is obviously smaller than that of steel A. The energy spectrum analysis shows that the precipitates are NbC, as shown in Figures 3(c) and (d). The second phase precipitates with the size distributed between 20 and 90 nm account for 90.6 percent. Those below 20 nm account for 8.2 percent, and those above 90 nm only account for 1.2 percent, as shown in Figure 4(b).

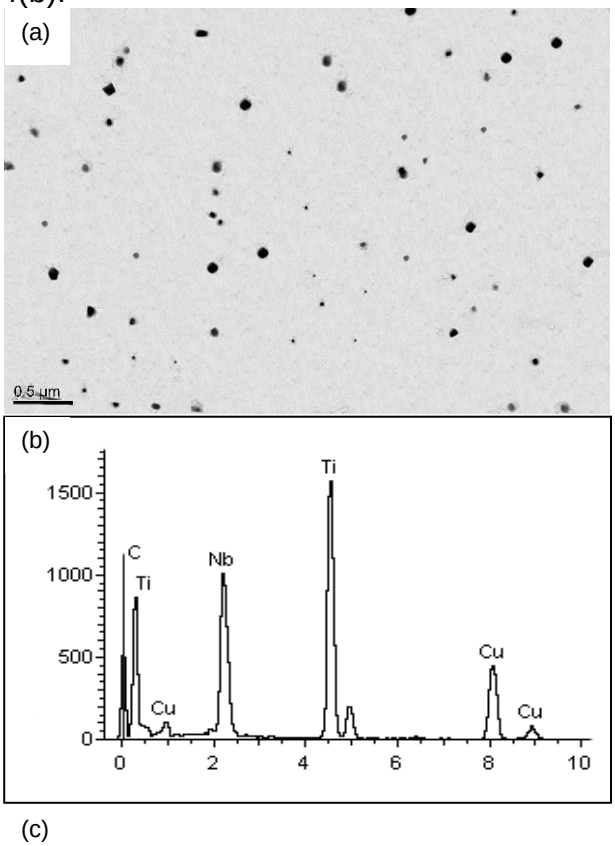

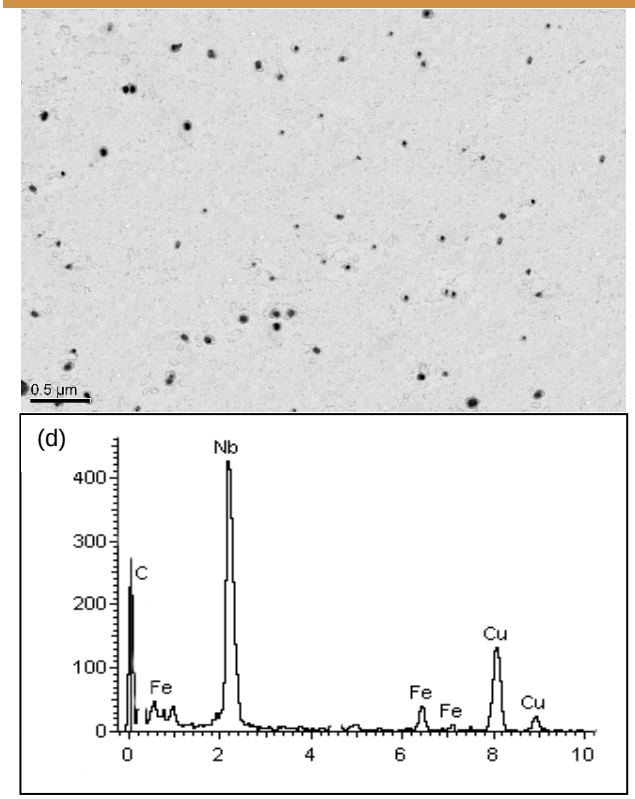

Figure 3. TEM images of the second phase precipitate of the tested steels (a) and (b) Steel A; (c) and (d) Steel B.

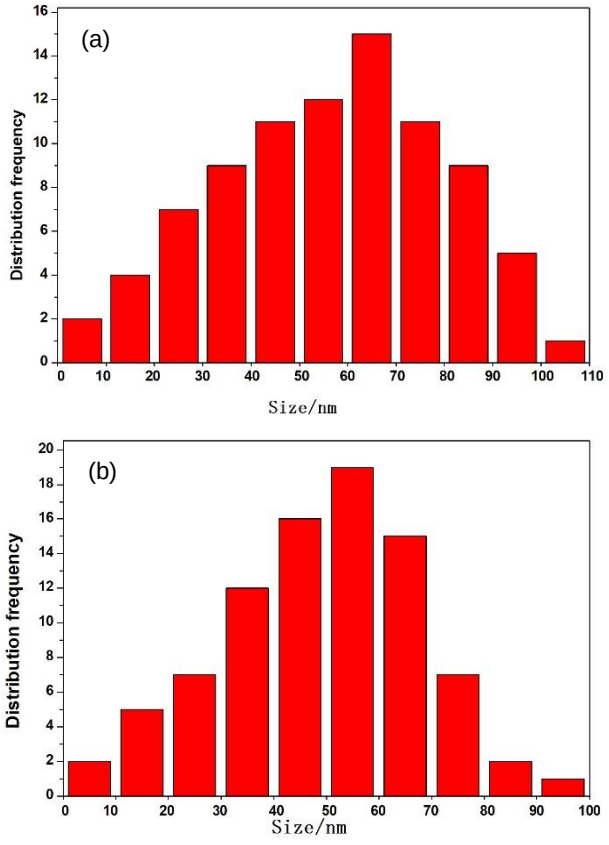

Figure 4. Size distribution of the second phase precipitates of the tested steels (a) Steel A; (b) Steel B.

3.5 Morphology of dislocation

The TEM images of the dislocation in the hot rolled steel plates and the surface position of square tube for steel A and steel B are shown in Figure 5. The morphology and density of dislocation in the two hot rolled plates are similar (Figure 5(a) and (b)). The dislocation in the ferrite is sparse, and distributes in intersected and entangled network. The density of the dislocation is about 0.2×10^{10} cm^{-2}, counted according to the definition of dislocation density [6]. Figure 5(c) and (d) show the morphology of the dislocation on the surface position of the square tubes for the tested steels. The density of the dislocation increased significantly. The dislocation distributes at the grain boundaries and the second phase precipitates. From the morphologies of the dislocations before and after tube forming, it is deduced that during the tube forming process, dislocations in different slip systems activated, with the initiation and proliferation of the dislocations, the density increased rapidly. Dislocations intertwined more and more severely, and the entangled regions evolved into individual cell structures. When the motived dislocations encounter obstacles (such as grain boundaries, the second phase precipitates, etc.), if the force for moving forward cannot overcome the pinning force of the obstacles, the dislocation that released by the same dislocation source would stop in front of the obstacles, resulting in the formation of a dislocation wall structure that hinders the motion of the dislocation. The density of dislocation is about $0.84*10^{10}$ cm^{-2} and $0.53*10^{10}$ cm^{-2} for steel A and steel B, respectively, as shown in Figure 5c, d.

Due to the complexity and non-uniformity of the deformation in the grain boundary region of polycrystalline material, the grain size has a significant effect on work hardening. Steels with fine grains has a greater work hardening than steels with coarse grains. To ensure the requirements

of further deformation for manufacturing square tube, it is necessary to control the degree of work hardening. Therefore, the ferrite grains should be ensured uniform and appropriate coarsening.

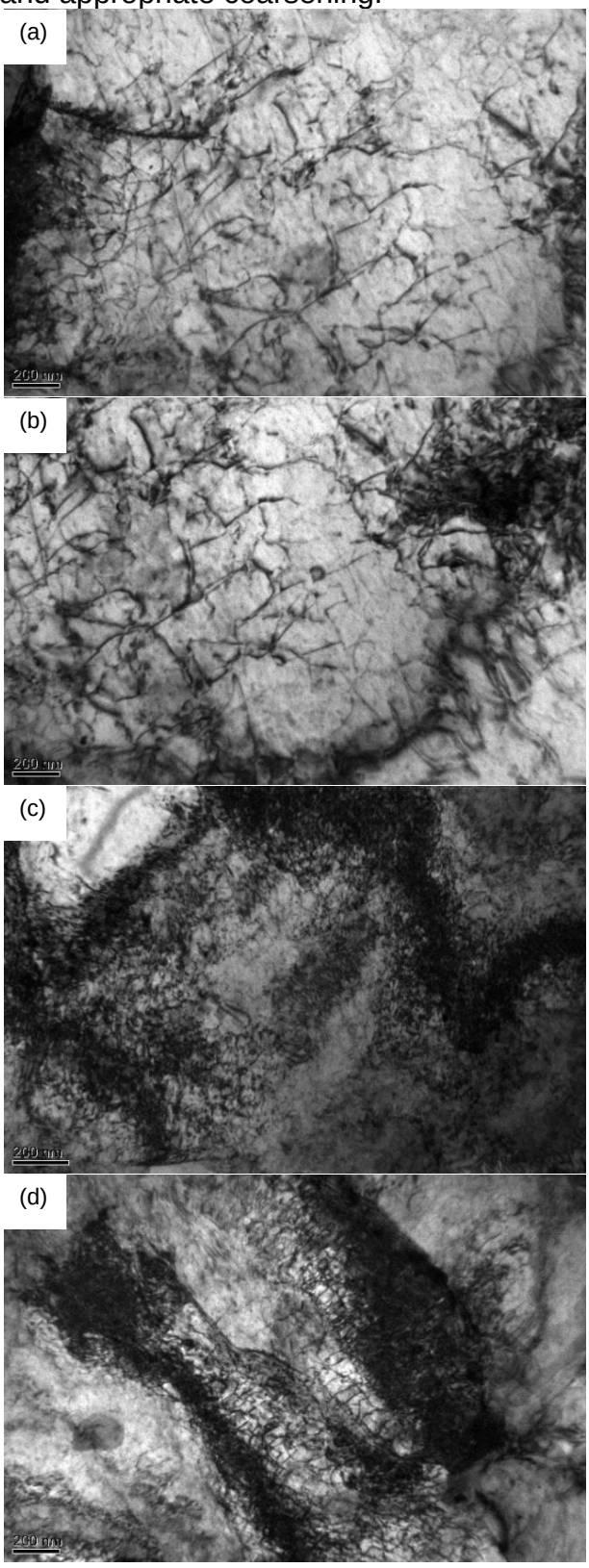

Figure 5. TEM images of the dislocation in the hot rolled steel plates and the surface position of square tube (a) plates of steel A; (b) plates of steel B; (c) square tube of steel A; (d) square tube of steel B.

3.6 Strengthening mechanism

In recent years, with the implementation of successive energy conservation and environmental protection policies, the demand for high strength square tube steels is more urgent than ever before. However, bending process is generally a necessary process for square tube manufacture, therefore, the plasticity is strictly required. The elongation of the hot rolled plate declined significantly because of the working hardening occurred in the complicated plastic tube forming process, and the higher the degree of work hardening, the greater the elongation reduction, and the greater the risk of cracking during bending of the square tube. Therefore, in order to ensure the processing performance of the square tube, it is necessary to control the degree of work hardening. Work hardening occurs in the plastic deformation below recrystallization temperature, during which strength and hardness increase and plasticity and toughness decline. There are two reasons for the occurrence of work hardening. On the one hand, the increase of the dislocation density in plastically deformation increases the shear stress required for the dislocation movement. On the other hand, many small crystal grains with chaotic lattice directions are generated on the slip surface and their grain boundaries are severe lattice distortion regions, which increase the slip resistance and the internal stress.

The changes in the mechanical properties after tube forming show that steel A has higher work hardening than steel B. The yield strength and tensile strength of steel A increase significantly, especially the yield strength, thus resulting in the yield ratio rising up to 0.92, and the elongation dropping by 6 percent. This performance is not conducive to further processing. The yield strength and tensile strength of steel B increase within 25MPa after tube

forming, the elongation decreases by 4.0 percent, and the yield ratio is 0.87, which is more conducive to further processing. The two steels show different degrees of work hardening that is decided by the difference of strengthening mechanism.

The yield strength can be predicted by the following equation [12]:

$$\sigma_y = \sigma_o + \Delta\sigma_s + \Delta\sigma_G + \Delta\sigma_{Dis} + \Delta\sigma_{Orowan} \quad (1)$$

Where σ_y is yield strength; $\Delta\sigma_0$ is lattice friction stress with the value of 48 MPa; $\Delta\sigma_s$, $\Delta\sigma_G$, $\Delta\sigma_{Orowan}$, and $\Delta\sigma_{Dis}$ are the strengthening factors caused by solid solution, grain refinement, precipitation and dislocation, respectively.

Solid solution hardening can be expressed as follows [12]:

$$\Delta\sigma_S = 4750[C] + 3750[N] + 84[Si] + 37[Mn] \quad (2)$$

Where [M] is the content of element M dissolving in ferrite. Si and Mn are ferrite-tube forming elements, all dissolved in ferrite. Precipitates fix all N element. The [C] content is about 0.011 percent and 0.018 percent respectively for steel A and steel B, calculated according to the formula of Nb and Ti solid solubility. Solid solution strengthening contributes about 95 MPa and 137 MPa for steel A and steel B, respectively.

Grain refinement hardening effect can be calculated by the well-known Hall–Petch equation [12]:

$$\Delta\sigma_G = k_y * d_F^{-1/2} \quad (3)$$

Where d_F is the average ferrite grain size; ky is a constant and its value is 17.4 MPa·mm$^{1/2}$. The calculation result shows that the grain refinement effect is 341 MPa and 286 MPa for steel A and steel B, respectively.

The essence of precipitation hardening lies in the hindering effect of second phase particles on the movement of dislocations. The well-known Ashby–Orowan model is widely used to calculate the precipitation hardening effect [12]:

$$\Delta\sigma_{Orowan} = 8.995\times10^3 * \frac{f^{1/2}}{d} * \ln(2.417d) \quad (4)$$

Where *f* is the volume fraction of precipitates and d is the mean diameter of precipitates. The theoretical density of steel A and steel B was 0.15 percent and 0.10 percent, respectively. The strengthening effect caused by the precipitates was 28 MPa and 30 MPa for steel A and steel B, respectively.

The dislocation strengthening can be estimated using the following equation [12] :

$$\Delta\sigma_d = \alpha * G * b * \rho^{1/2} \quad (5)$$

Where is a constant depending on the crystal structure, (for steel,) α= 0.435. G is shear modulus, and G= 8.3×104 MPa. b is the burgers vector of a dislocation with a value of 0.248×10^{-7} cm; ρ is the dislocation density in 1/cm^2. The average ρ is about 0.2×10^{10} cm^{-2} estimated by the number of dislocations in thin regions of the TEM foils. Thus, the strengthening contribution of dislocations was about 40 MPa for steel A and steel B before roll tube forming. The average ρ was about 0.84×10^{10} cm^{-2} and 0.53×10^{10} cm^{-2} for steel A and steel B, respectively, so the strengthening contribution of dislocations was 82 MPa and 65 MPa for steel A and steel B, respectively.

Figure 6 shows the calculated components for yield strength for the tested steel A and steel B before and after tube forming. It can be seen that the calculated value is close to the actual measured value. The calculation shows the grain refinement strengthening contributes the most to the yield strength, which account for 61.8 percent and 52.9 percent for steel A and steel B, respectively. The solid solution strengthening was the second prominent strengthening mode, accounting for 17.2 percent and 25.3 percent for steel A and

steel B, respectively. Precipitation strengthening and dislocation strengthening contributed little to the yield strength. The composition, the second phase precipitates, and the content of solid solution elements remained unchanged after the manufacture of the square tube, except for the increase of the dislocation density. After tube forming, the increments of dislocation strengthening reached 82 MPa (Steel A) and 65 MPa (Steel B), respectively, which account for 13.8 percent (Steel A) and 11.3 percent (Steel B) of the total yield strength, respectively, and increase by 42 MPa (Steel A) and 25 MPa (Steel B) respectively compared with the hot rolled plates. The contribution of dislocation strengthening for steel A is significantly higher than that of steel B. Therefore, the comprehensive mechanical properties of steel B are more suitable for manufacturing automotive square tube by secondary tube forming.

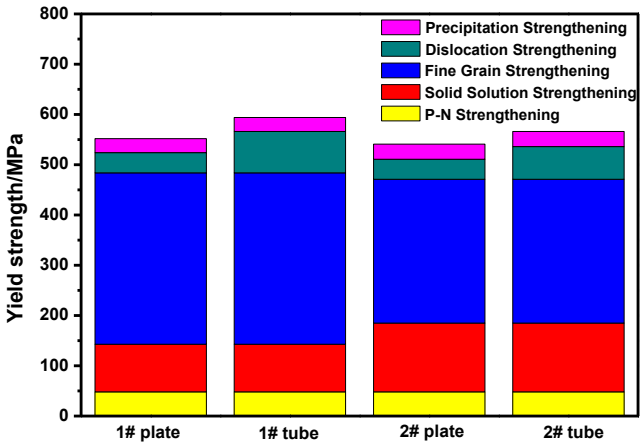

Figure 6. Yield strength and its component of the tested steels before and after tube forming.

4 CONCLUSION

The microstructure, properties, and strengthening mechanism of 600MPa grade high ductility hot-rolled sheet steel were investigated by utilizing OM, SEM and TEM. The following results are obtained.

(1) The microstructures of the tested steels are composed of ferrite and a small amount of pearlite. Compared with the high C-high Mn-Nb microalloyed steel, the size of the ferrite and pearlite of low C-low Mn-Nb and Ti microalloyed steel is finer, while the size of the second phase precipitates is larger.

(2) The mechanical properties of the tested steels are similar before tube forming, except that the yield ratio of the low C-low Mn-Nb and Ti microalloyed steel is higher. The low C-low Mn-Nb and Ti microalloyed steel exhibits significantly work hardening after tube forming, the yield strength and tensile strength increase by 45 MPa and 26 MPa, respectively, and the elongation decrease by 6.0 percent. The yield strength and tensile strength of the high C-high Mn-Nb microalloyed steel increase by 22 MPa and 10 MPa, and the elongation decrease by 4.0 percent.

(3) Grain refinement strengthening is the prominent strengthening mode, accounting for 52.9 percent in low C-low Mn-Nb and Ti microalloyed steel and 61.8 percent in high C-high Mn-Nb microalloyed steel, respectively. Solid solution strengthening is the second main strengthening mode, accounting for 17.2 percent in low C-low Mn-Nb and Ti microalloyed steel and 25.3 percent in high C-high Mn-Nb microalloyed steel.

(4) The dislocation strengthening increase to 82 MPa of the low C-low Mn-Nb and Ti microalloyed steel after tube forming, which is higher than that of the high C-high Mn-Nb microalloyed steel. The high C-high Mn-Nb microalloyed steel has a relatively low work hardening rate, which is more suitable for manufacturing automotive square tube for secondary tube forming.

REFERENCES

1 SPENCE M A，ROSCOE C V. Bi-metal CRA-lind pipe employed for North Sea field development [J]. Oil＆Gas Journal，1999，97（18）：80-88.

2 CHEN W C，PETERSEN C W. Corrosion performance of welded CRA-lined pipes for flow lines [J]. SPE Production Engineering，1991，7（4）：375-378.

3 RUSSELL D K，WILHELM S M. Analysis of bimetallic pipe for sour service [J]. SPE Production Engineering，1991，6（3）：291-296.

4 Zhang P C, Wu H B, Tang D, et al. Dissolving behaviors of carbonitrides in Nb-V-Ti and C-Ti microalloying steels [J]. Acta. Metall. Sin., 2007, 43(7): 753-758.

5 Nishio, Shinj. Investigation of car body structural optimization method [J]. International Journal of Vehicle Design, 1990, 11(1): 79-86.

6 Yoshimura, Masatakal, Nishiwaki. A multiple cross-sectional shape optimization method for automotive body flames [J]. Journal of Mechanical Design, 2005, 127(1):49-57.

7 Botkin. Structural optimization of automotive body components based on parametric solid modeling [J]. Engineering with Computers, 2002, 18(2):109-115.

8 Kang，Choi．Design sensitivity analysis of body structure using skeleton model [J]. Proceedings of the 6th International Pacific Conference on Automotive Engineering，1991:525-531, Korea.

9 Shin, Lee, Song, Park. Automotive door design with the ULSAB concept using structural optimization [J]. Structural and Multidisciplinary Optimization, 2002, 23(4):320-327.

10 Hong S G, Kang K B, Park C G. Strain-Induced Precipitation of NbC in Nb and Nb-Ti Microalloyed HSLA Steels [J]. Scripta Mate., 2002, 46(5):163-170.

11 Thillou V. Basic Metal Processing Research Institute Report, University of Pittsburgh, PA, USA, 1997.

12 Pickering F B. Physical Metallurgy and the Design of Steels. London: Applied Science Publishing Ltd., 1978: 63